

## Broadband magnetic losses of nanocrystalline ribbons and powder cores



Cinzia Beatrice<sup>a,\*</sup>, Samuel Dobák<sup>b</sup>, Enzo Ferrara<sup>a</sup>, Fausto Fiorillo<sup>a</sup>, Carlo Ragusa<sup>c</sup>, Ján Füzér<sup>b</sup>, Peter Kollár<sup>b</sup>

<sup>a</sup> Istituto Nazionale di Ricerca Metrologica, Nanoscience and Materials Division, Torino, Italy

<sup>b</sup> Institute of Physics, Faculty of Science, P.J. Šafárik University, Košice, Slovakia

<sup>c</sup> Politecnico di Torino, Energy Department, Torino, Italy

### ARTICLE INFO

#### Article history:

Received 30 May 2016

Accepted 22 July 2016

#### Keywords:

Nanocrystalline alloys

Magnetic losses

High-frequency losses

Landau–Lifshitz equation

### ABSTRACT

Finemet type alloys have been investigated from DC to 1 GHz at different induction levels upon different treatments: as amorphous precursors, as ribbons nanocrystallized with and without an applied saturating field, as consolidated powders. The lowest energy losses at all frequencies and maximum Snoek's product are exhibited by the transversally field-annealed ribbons. This is understood in terms of rotation-dominated magnetization process in the low-anisotropy material. Intergrain eddy currents are responsible for the fast increase of the losses with frequency and for early permeability relaxation of the powder cores. Evidence for resonant phenomena at high frequencies and for the ensuing inadequate role of the static magnetic constitutive equation of the material in solving the magnetization dynamics via the Maxwell's diffusion equation of the electromagnetic field is provided. It is demonstrated that, by taking the Landau–Lifshitz–Gilbert equation as a constitutive relation, the excellent frequency response of the transverse anisotropy ribbons can be described by analytical method.

© 2016 Elsevier B.V. All rights reserved.

## 1. Introduction

Nanocrystalline Finemet-type alloys combine high magnetic softness and versatility with excellent broadband response, comparable or even superior, in terms of permeability and loss behavior, to the one offered by soft ferrites [1–3]. Once reduced in powder form and consolidated as conventional ring samples, they may exhibit nearly flat permeability response up to a few hundred MHz [4,5]. But, while faced with a wide range of applications [6], these materials display a poorly assessed broadband behavior, where the analysis is, as in the case of amorphous alloys, mostly qualitative and generally limited to the description of the frequency dependence of the initial permeability [5,7,8]. Quantitative description and prediction of magnetic permeability and energy loss behavior in metallic alloys up to radiofrequencies are indeed difficult objectives and drastic approximations are usually required. Permeability and impedance of planar magnetic conductors have, for example, been calculated disregarding the role of the domain walls (d.w.s) and assuming linear response by the rotational processes [9,10]. Thanks to these approximations one can actually perform the analysis of eddy currents at microwave

frequencies by taking the Landau–Lifshitz–Gilbert (LLG) equation as the constitutive magnetic relation of the material in the description of electromagnetic field diffusion by the Maxwell's equations [11,12]. Wishing, however, to assess the material response both at high and low frequencies, one should additionally take into account the d.w. processes, the sole source of the quasi-static energy loss and responsible for the generation of dynamic loss in excess of the one predictable according to a homogeneous d.w. free magnetization process [13]. This feat has not been accomplished yet.

In this paper we discuss a comprehensive experimental investigation on the DC–1 GHz behavior of permeability and energy losses, measured at defined peak polarization levels ( $0.5 \text{ mT} \leq J_p \leq 200 \text{ mT}$ ), of the  $\text{Fe}_{73}\text{Nb}_3\text{Cu}_1\text{Si}_{16}\text{B}_7$  (Finemet) nanocrystalline alloy. Both tapewound and consolidated powder ring samples have been measured. Best broadband response is obtained with ribbons nanocrystallized and cooled under a saturating transverse DC magnetic field, a feature associated with a relatively sharp transverse domain structure, leading to prevalence of the rotational magnetization processes. It is shown that the standard analysis based on the statistical theory of losses permits us to apply, in general, the usual concept of loss separation, also in the presence of skin effect, up to some hundred kHz. By keeping, in particular, the induction values sufficiently low, as required in most high-frequency applications, the condition of quasi-linearity

\* Corresponding author.

E-mail address: [c.beatrice@inrim.it](mailto:c.beatrice@inrim.it) (C. Beatrice).

of the DC magnetic constitutive equation is satisfied and a standard equation for the classical loss component applies. Entering, however, the MHz range, where the diffusion of the electromagnetic field interferes on a same time scale with the spin dynamics, a dynamic constitutive relation is expected to emerge and govern the dissipation of the magnetic energy. Such a relation is generally unknown, although one could imagine retrieving it by solution of an inverse problem. We show, however, that the especially interesting case of the low-loss transverse anisotropy ribbons, with their weakly contributing transverse d.w.s, can be treated describing the magnetic constitutive relation through the Landau–Lifshitz equation. Such an approach, substantiated by experimental evidence of magnetic resonance effects, is pursued by an analytical procedure and permits one to provide broadband fitting of the measured energy loss.

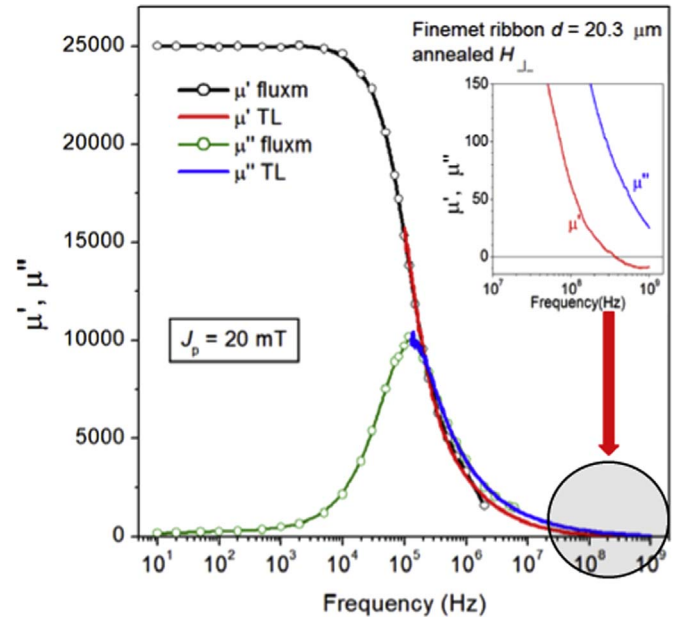
## 2. Experimental procedure and basic results

Tapewound 18 mm diameter ring samples were prepared with 10 mm wide 20  $\mu\text{m}$  thick  $\text{Fe}_{73}\text{Nb}_3\text{Cu}_1\text{Si}_{16}\text{B}_7$  precursor amorphous ribbons, obtained by planar flow casting and encased in boron nitride toroidal holders. No tensile stress was applied to the ribbon during winding, the number of layers varying between 3 and 10 from sample to sample. Nanocrystallization annealing, performed at 550  $^\circ\text{C}$ , was followed by slow cooling to room temperature, with and without an applied saturating DC field. Either circumferential ( $H_{||}=300\text{ A/m}$ ) or transverse ( $H_{\perp}=15\text{ kA/m}$ ) fields were applied, in order to induce longitudinal/transverse anisotropy. Composite ring samples (outside diameter 10 mm, inside diameter 5 mm, thickness 3.3 mm) were also prepared, as described in [8], by pulverization of the precursor ribbon at either room temperature or liquid nitrogen temperature, powder consolidation, and nanocrystallization annealing. Particles of size 20–150  $\mu\text{m}$  were produced by cryomilling (sample L), smaller on the average with respect to the particles (50–300  $\mu\text{m}$ ) obtained by milling at room temperature (sample R). The resistivity values of the composites, approximately doubled with respect to the resistivity of the alloy ( $256 \cdot 10^{-8}\ \Omega\text{ m}$  in sample R and  $273 \cdot 10^{-8}\ \Omega\text{ m}$  in sample L versus  $121 \cdot 10^{-8}\ \Omega\text{ m}$ ), point to good interparticle contact and nearly homogeneous bulk conduction. The magnetic characterization of the ring samples was performed by fluxmetric measurements at defined peak polarization level  $J_p$  up to 10 MHz. A transmission line (TL) method using a Vector Network Analyzer (Agilent 8753 A) and TEM wave power  $P_{\text{TL}}=10\text{ mW}$  on a short circuited coaxial line was instead adopted in the range  $100\text{ kHz} \leq f \leq 1\text{ GHz}$  [14]. It is shown that, as far as a quasi-linear response of the material applies, the measured high-frequency real  $\mu'$  and imaginary  $\mu''$  permeability components are independent of  $P_{\text{TL}}$  (i.e.  $J_p$ ) [15] and one obtains the energy loss at a given  $J_p$  value as

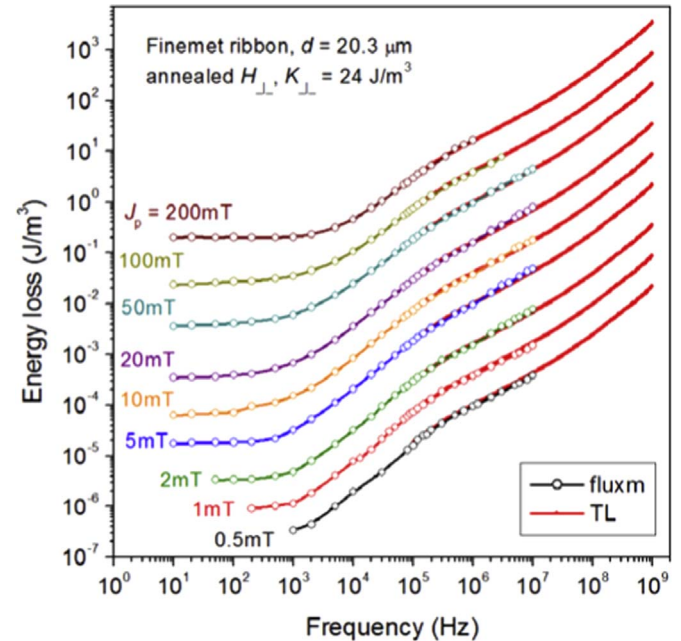
$$W(J_p, f) = \pi J_p^2 \mu''(f) / (\mu'^2(f) + \mu''^2(f)) [J/m^3]. \quad (1)$$

Fig. 1 provides an example of experimental  $\mu'$  and  $\mu''$  dependence on frequency in the transverse anisotropy  $K_{\perp}$  ( $H_{\perp}$  annealed) ribbons, where the fluxmetric measurements (symbols), taken up to a few MHz at  $J_p=20\text{ mT}$ , are observed to seamlessly connect to the high-frequency TL results, a property ensuing from the linear response of the material. This finding is corroborated by magneto-optical Kerr experiments, showing that the d.w. processes are progressively inhibited with increasing the frequency towards the MHz range, leaving room for the linear magnetization rotations [16]. It is notably observed in Fig. 1 (see inset) that  $\mu'(f)$  attains negative values beyond some hundred MHz and the related dispersion behavior points to magnetic resonance phenomena.

An overall view of the DC – 1 GHz  $W(J_p, f)$  behavior of the  $K_{\perp}$



**Fig. 1.** Real  $\mu'$  and imaginary  $\mu''$  permeability components versus frequency measured in the transverse anisotropy Finemet ribbon of thickness  $d=20.3\ \mu\text{m}$ . The fluxmetric measurements (symbols) are performed at a defined peak polarization value  $J_p=20\text{ mT}$  up to a few MHz. The transmission line (TL) results (continuous lines), obtained in the upper frequency range with TEM wave power  $P_{\text{TL}}=10\text{ mW}$ , coincide with the fluxmetric measurements beyond a few hundred kHz. The passage of  $\mu'$  through negative values beyond a few hundred MHz (see inset) points to resonant dispersion associated with the rotational processes.



**Fig. 2.** Energy loss  $W(f)$  versus frequency up to  $f=1\text{ GHz}$  in the transverse anisotropy nanocrystalline ribbon.  $W(f)$  is directly measured at given peak polarization value  $J_p$  by the fluxmetric method up to the maximum frequency  $f=10\text{ MHz}$  (symbols). By the transmission line (TL) method one gets, starting from a few hundred kHz, the real  $\mu'(f)$  and imaginary  $\mu''(f)$  permeability components at defined TEM wave power.  $W(f)$  is then calculated for any  $J_p$  value by Eq. (1) (continuous lines). The two methods provide matching  $W(f)$  values in the overlapping frequency interval.

ribbons, with  $J_p$  ranging between 0.5 mT and 200 mT, is provided in Fig. 2, where the fluxmetric measurements are shown to smoothly superpose, for all  $J_p$  values, to the TL results at intermediate frequencies. It is stressed that by

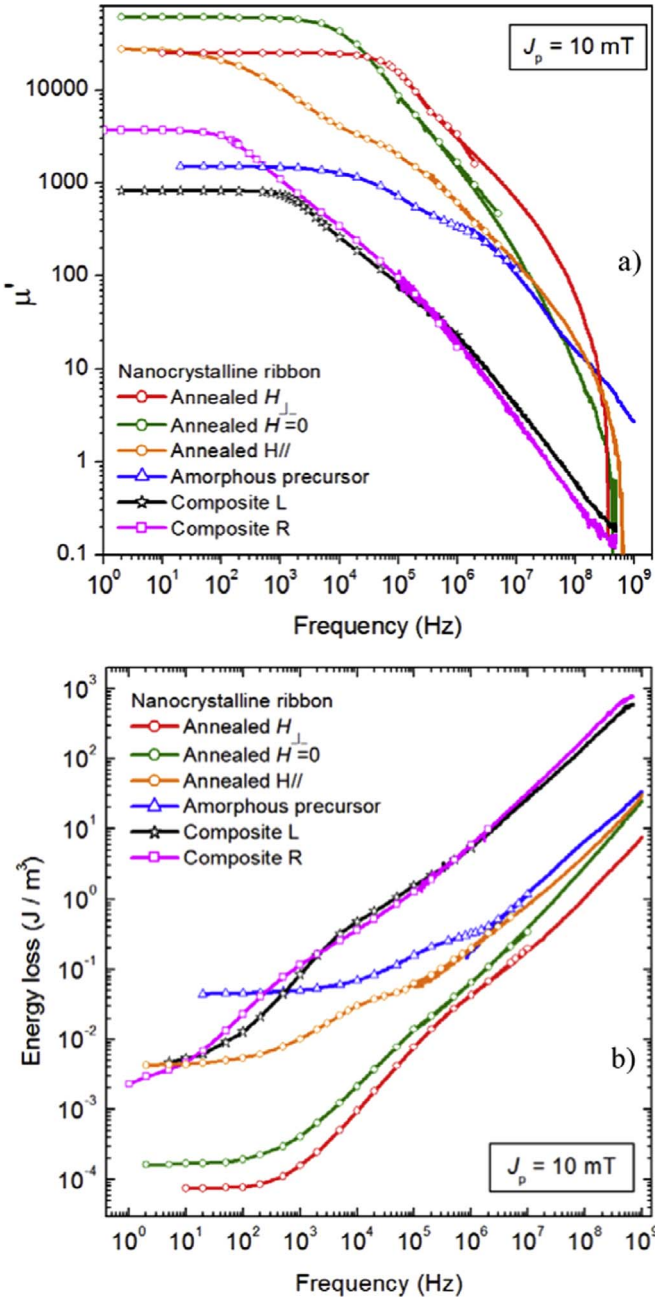


**Fig. 3.** Real permeability component  $\mu'$  (a) and energy loss  $W(f)$  (b) measured at  $J_p = 10$  mT in the investigated nanocrystalline alloys up to 1 GHz. Symbols and continuous lines refer to the fluxmeter and TL measuring methods, respectively. The highest Snoek's product (a) and the lowest energy losses are obtained in the transverse anisotropy ( $H_\perp$  annealed) ribbons. More or less conspicuous double relaxation effect is observed in all cases, pointing to some discontinuity with frequency of the magnetic constitutive equation.

the TL method we actually measure  $\mu'(f)$  and  $\mu''(f)$  associated with  $J_p$  value decreasing with frequency, according to  $J_p(f) = \sqrt{(2P_{TL}/Z_0) \cdot (\mu'^2(f) + \mu''^2(f))} / \pi <r>$ , where  $Z_0$  is the characteristic impedance of the line and  $<r>$  is the average radius of the ring sample. In the present case  $J_p$  is found to decrease from the value 15 mT at 100 kHz to about 0.023 mT at 1 GHz. But the linear response of the material ensures that the actual energy loss dissipated at given  $J_p$  can be calculated by Eq. (1), as shown by the array of broadband energy loss curves of Fig. 2.

A comparative example of the frequency dependence of permeability and loss exhibited at given  $J_p$  by the differently treated

nanocrystalline materials, including the precursor amorphous alloy and the composite rings, is provided in Fig. 3. The highest Snoek's product ( $\mu_{DC} \cdot f_c = 3.7 \cdot 10^9$  Hz, with  $f_c$  the cutoff frequency, at  $J_p = 10$  mT) and the lowest energy loss at all frequencies is exhibited by the  $K_\perp$  ribbons. This property stems from the dominant rotational character of the involved magnetization process, in combination with the low anisotropy value  $K_\perp = 24$  J/m<sup>3</sup> (anisotropy field  $H_k = 38.4$  A/m). A more or less important contribution by the d.w. processes occurs in the other differently treated samples and is the cause of the large scatter of the associated quasi-static loss values. But this contribution may suffer a strong evolution upon increasing frequencies. We might generally say, in all cases, that a dynamic magnetic constitutive equation could be a better substitute for the conventional DC one at sufficiently high frequencies.

### 3. Loss decomposition towards high-frequencies

The standard approach to the loss analysis based on the simple analytical formulations offered by the Statistical Theory of Losses (STL) and the related concept of loss decomposition [13] is broadly applied in the assessment of the properties of magnetic steel sheets at power frequencies. The STL is shown to comply, in general, with the experiments up to frequencies where the skin effect strongly enters into play. Beyond such limit more complex formulations, exploiting hysteresis modeling (such as the Dynamic Preisach Model) and numerical calculations are usually employed [17,18]. However, in experiments aiming at the magnetic behavior of the material up to radiofrequencies, starting from quasi-static characterization, we are naturally bound to the low induction regimes, where quasi-linear DC constitutive equation can often be assumed and the concept of energy loss can also be viewed in terms of complex permeability. This approximation seems well justified, for example, when operating inside the Rayleigh region, where the peak permeability and the averaged differential permeability coincide. Consequently we are enabled to express the eddy current classical loss component in the ribbon samples through the standard formula [13]

$$W_{\text{class}}(f) = \frac{\pi}{2} \cdot \frac{\lambda J_p^2}{\mu_{DC}} \cdot \frac{\sinh \lambda - \sin \lambda}{\cosh \lambda - \cos \lambda}, \quad [J/m^3] \quad (2)$$

where  $\lambda = \sqrt{\pi \sigma \mu_{DC} d^2 f}$ ,  $\sigma$  is the material conductivity and  $d$  is the ribbon thickness. Eq. (2) can be applied also to bulk samples having rectangular cross-section by posing  $\lambda = \sqrt{\pi \sigma \mu_{DC} 12k(R)S f}$ , where  $S$  is the cross-sectional area and  $k(R)$  is a function of the aspect ratio  $R$  [19]. The here investigated composite rings have  $S = 2.5 \text{ mm} \times 3.3 \text{ mm}$  and  $k(R) = 0.0325$ . The experimental  $W(f)$  behavior measured in the composite R is shown in Fig. 4a.

The fluxmetric and TL results coincide upon the overlapping frequency band (100 kHz–10 MHz) up to about  $J_p = 50$  mT, beyond which a deviation from linear behavior of the constitutive equation occurs. Near-homogeneous macroscopic eddy current patterns are envisaged in these composites, as suggested by the comparison of the experimental  $W(f)$  curves with the classical loss curves calculated with Eq. (2).  $W(f)$  is then fully described by the so obtained  $W_{\text{class}}(f)$  at intermediate frequencies, the lower the  $J_p$  value the broader the frequency interval upon which experiments and classical prediction coincide. In fact, by increasing  $J_p$ , the contribution to the magnetization process by the d.w. displacements, which is the source of the hysteresis  $W_h$  and the excess loss  $W_{\text{exc}}$  contributions, is made to increase and on going towards quasi-static conditions the related dissipation effects largely overcome the purely classical ones associated with the rotations.



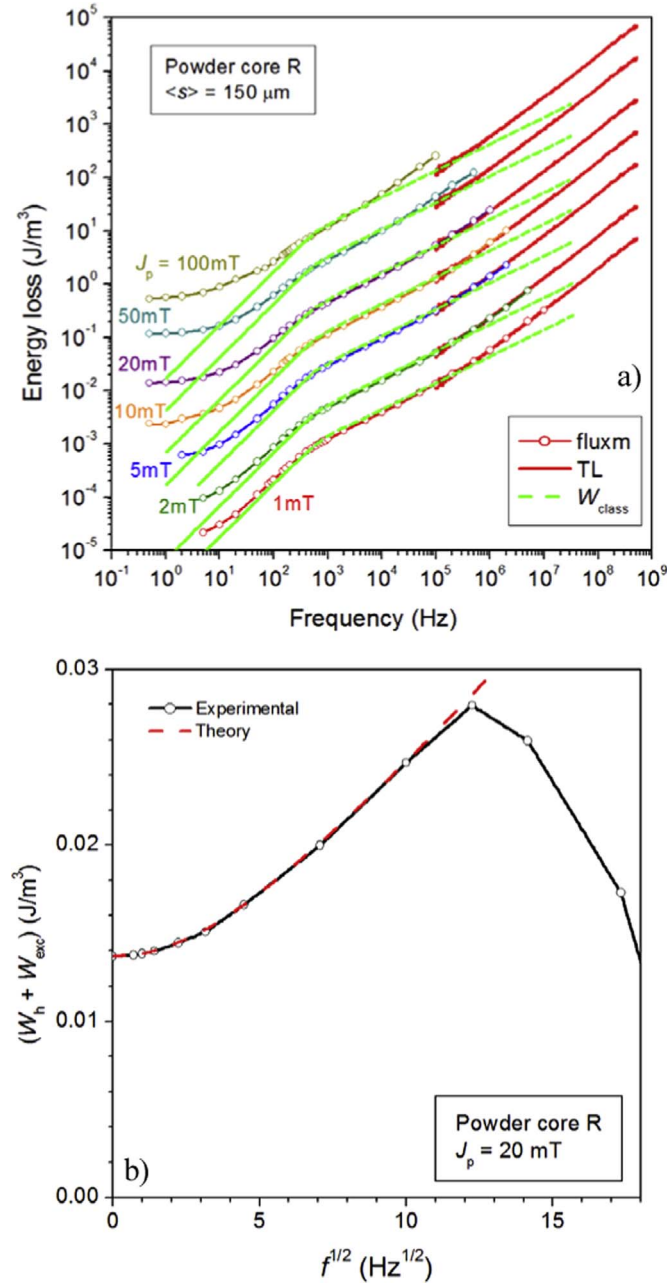


**Fig. 4.** a) Energy loss  $W(f)$  versus frequency in the consolidated nanocrystalline core (particle size ranging between  $50 \mu\text{m}$  and  $300 \mu\text{m}$ ). The fluxmetrically and TL measured losses coincide in the experimental overlapping frequency range up to about  $J_p = 50$  mT, where the magnetic constitutive equation is expected to significantly depart from linearity. The dashed lines show the behavior of the classical loss  $W_{\text{class}}(f)$ , calculated with Eq. (2) for the specific case of a bulk ring sample. b) Example of loss decomposition in the low frequency range ( $J_p = 20$  mT). The quantity  $W_h + W_{\text{exc}}(f)$  (symbols), obtained as  $W(f) - W_{\text{class}}(f)$  is compared with the prediction by Eq. (3) (dashed line).

This is put in evidence by the departure of the  $W(f)$  curves from the predicted  $W_{\text{class}}(f)$  below a few hundred Hz. On the other hand, on entering the MHz range,  $W(f)$  starts to follow a power law different from the  $f^{1/2}$  law predicted by Eq. (2). It is concluded that at such frequencies the constitutive equation, though linear, has evolved with respect to  $\mu_{\text{DC}}$ . Up to this limit, however, we are basically able to assess the  $W(f)$  behavior by STL and loss separation, with the role of the skin effect accounted for by use of Eq. (2). We thus find  $W_h$  by extrapolating  $W(f)$  to  $f \rightarrow 0$  and the experimental excess loss as  $W_{\text{exc}}(f) = W(f) - W_{\text{class}}(f) - W_h$ . This quantity is

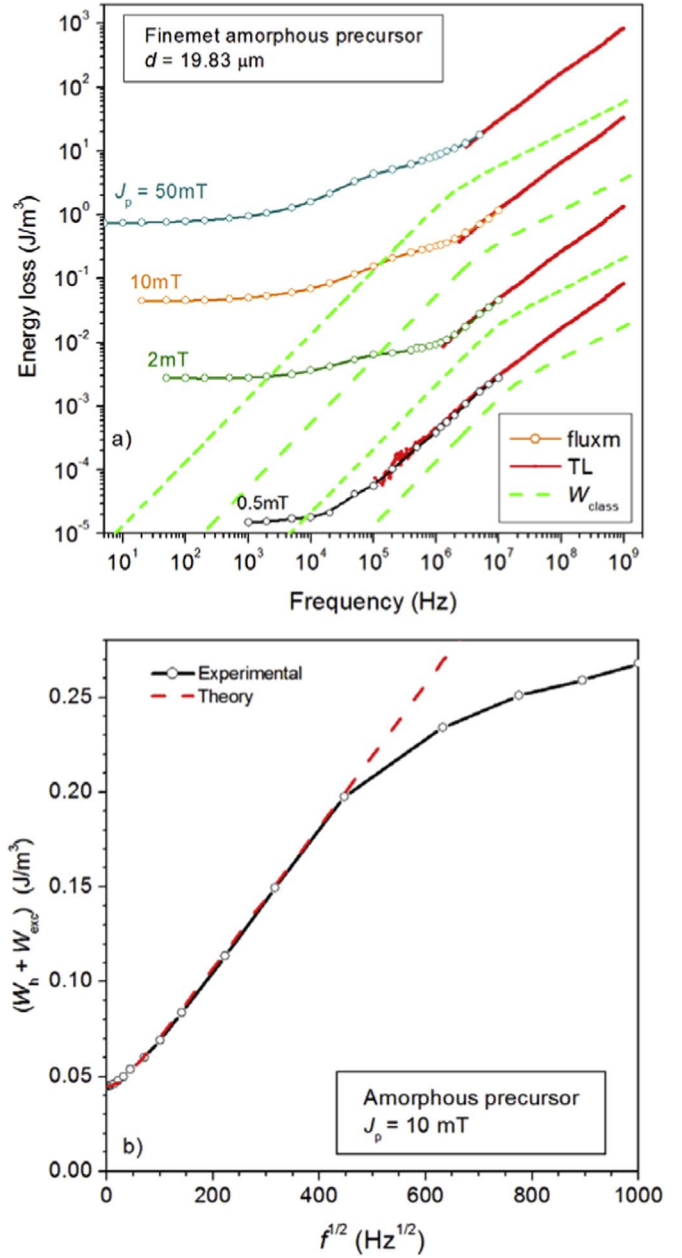


**Fig. 5.** a) Energy loss  $W(f)$  versus frequency in the Finemet amorphous precursor at different  $J_p$  values. The fluxmetric and TL results superpose upon narrower frequency interval on increasing  $J_p$ , because of the increasing role of the d.w. processes. The classical loss  $W_{\text{class}}(f)$  (dashed lines) is calculated with Eq. (2). b) The behavior of the experimental quantity  $W_h + W_{\text{exc}}(f) = W(f) - W_{\text{class}}(f)$ , with  $W_{\text{class}}(f)$  given by Eq. (2), is well described by Eq. (3) up to  $f \sim 200$  kHz.

calculated by the expression

$$W_{\text{exc}}(f) = 2n_0V_0J_p \cdot \int_0^{\pi/2} \left( \sqrt{1 + \frac{8\sigma GSV_0\pi f J_p \cos\phi}{n_0^2V_0^2}} - 1 \right) \cos\phi d\phi \quad (3)$$

$[\text{J/m}^3]$

where  $G = 0.1356$  and  $n_0$  and  $V_0$  are two statistical parameters related to the distribution of the local threshold fields for magnetization reversal across the sample cross-section [20]. These local fields are, in particular, associated with physical entities, the magnetic objects, a number  $n$  of them being active at a given instant of time, typically according to a linear law  $n = n_0 + H_{\text{exc}}/V_0$ , with  $H_{\text{exc}} = W_{\text{exc}}/4J_p$  and  $n = n_0$  for  $f = 0$ . Eq. (3) predicts  $W_{\text{exc}}(f) \propto f^{1/2}$  for  $n \gg n_0$ , that is, at sufficiently high frequencies. It is shown to

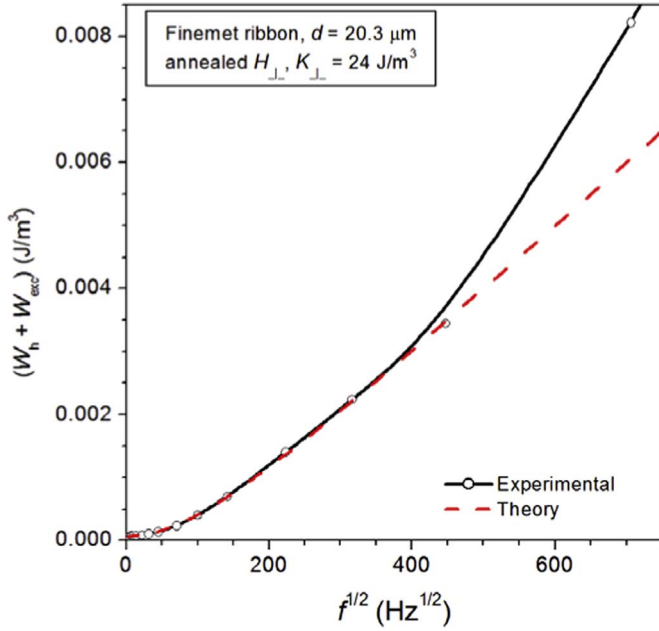


**Fig. 6.** The experimental quantity  $W_h + W_{\text{exc}}(f)$  in the transverse anisotropy Finemet ribbon is predicted by Eq. (3) up to  $f \sim 200$  kHz.

faithfully describe (Fig. 4b) the experimental frequency dependence of  $W_{\text{exc}}(f)$  in the composite material up to about  $f = 150$  Hz (with constant  $W_h$  value). Beyond this frequency both  $W_h$  and  $W_{\text{exc}}(f)$  undergo, because of d.w. relaxation and prevalence of rotations, a rapid decrease, to disappear at a few hundred Hz. A same analysis performed on the amorphous precursor ribbon by calculating  $W_{\text{class}}(f)$  with Eq. (2), is illustrated in Fig. 5. A major role is played here by the d.w. processes and  $W_{\text{class}}(f)$  never comes close to the measured loss. The quantity  $W_h + W_{\text{exc}}(f) = W(f) - W_{\text{class}}(f)$ , shown versus  $f^{1/2}$  at  $J_p = 10$  mT in Fig. 5b, fits into the prediction of Eq. (3) (dashed line) up to about 200 kHz. The standard approach to loss decomposition applies then up to this frequency, a conclusion drawn also for the transverse anisotropy  $K_{\perp}$  ribbons, as illustrated by the comparison of the related experimental and predicted  $W_h + W_{\text{exc}}(f)$  behaviors in Fig. 6.

The analysis of the longitudinally field annealed ribbons, endowed with a system of longitudinal  $180^\circ$  d.w.s, and of the ribbons nanocrystallized in the absence of magnetic field, characterized by a relatively complex domain structure, leading to admixture of d. w. and rotational processes [21], showed that the number  $n$  of active magnetic objects followed a law of the type  $n = n_0 + (H_{\text{exc}}/V_0)^{1/2}$ , leading to a formulation for  $W_{\text{exc}}(f)$  fairly more complex than Eq. (3). This provides, in conjunction with Eq. (2), good agreement with the experimental loss up to about 10 kHz in the longitudinal anisotropy ribbons and 400 kHz in the near-zero anisotropy ones.

### 3.1. An analytical approach to the energy loss in the transverse anisotropy ribbons

The previous analysis brings to light the substantial limitations of the theoretical assessment of magnetic losses at high frequencies in conducting soft magnets. We have previously shown that, even by assuming very low-induction values and calculating the classical losses under linear constitutive equation, we attain good predicting capability up to a few hundred kHz at most. This limit falls down to about 10 kHz in the longitudinal anisotropy ribbons, where the magnetization process proceeds exclusively by the d.w. displacements. We actually expect that coupling between eddy currents and spin dynamics occurs at high frequencies, an

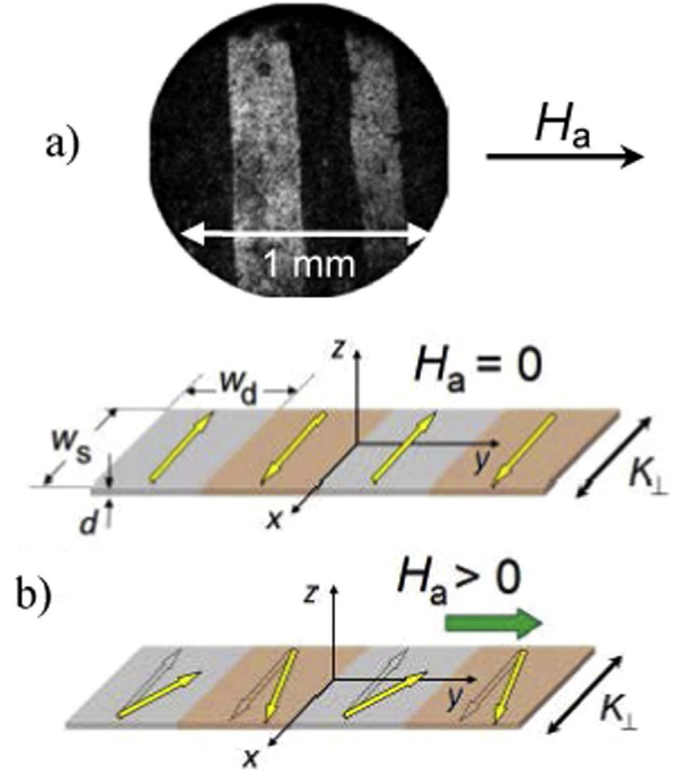


**Fig. 7.** Observed domain structure in the  $K_{\perp}$  nanocrystalline ribbon (a) and its schematic representation (b). The magnetic moments inside the transverse domains oscillate around the  $x$ -direction upon application of a longitudinal ( $y$ -axis) AC field  $H_a$ .

effect possibly accounted for by use of an appropriate dynamic magnetic constitutive equation [11,12]. It is indeed observed, as sketched in the example of Fig. 1, that the dispersion of the complex permeability at the highest frequencies is consistent, in all the investigated materials, with resonant spin behavior. Thus, we might describe the oscillating response to an electromagnetic field of the spins inside the magnetic domains of the nanocrystalline ribbons by means of the Landau–Lifshitz equation, invoked as a dynamic constitutive equation. The problem appears quite simplified in the interesting case of  $K_{\perp}$  ribbons, which display the lowest losses at all frequencies and  $J_p$  values and the highest Snoek's product (see Fig. 3). Given the relatively sharp transverse domain structure induced in these samples, an example of which is given in Fig. 7a, the magnetization will change under an oscillating longitudinal field almost completely by spin rotation, as schematically shown in Fig. 7b.

While negligibly contributing to  $J_p$ , the d.w.s are set in motion by the applied field through an indirect magnetostatic effect and are the source of hysteresis and excess dynamic losses [16]. Spin rotations are a homogeneous process and are naturally associated with a classical loss model, which can be implemented in a relatively simple way exploiting the uniaxial character of the induced anisotropy and the related symmetry of the problem. In a previous approach to the broadband properties of  $K_{\perp}$  amorphous alloys, the description of the spin dynamics and the calculation of the classical loss by coupled Landau–Lifshitz and Maxwell's diffusion equations was performed by a numerical method [15,22]. In this Section we show that a similar approach can be pursued by an analytical procedure, by which a closed expression for the classical loss is eventually derived.

Let us therefore consider in the ribbon of width  $w_s$  and thickness  $d$  the antiparallel domain structure shown in Fig. 7b. Under an alternating field  $\mathbf{h}_a$  directed along the ribbon length ( $y$  axis) the

magnetization  $\mathbf{M}(z)$  ( $-d/2 \leq z \leq d/2$ ) oscillates around the easy axis  $x$ . Given the symmetry of the problem, no free poles are created at the (stationary) walls. The starting point of our analysis is the Landau–Lifshitz–Gilbert equation [22]

$$\frac{\partial \mathbf{M}}{\partial t} = -\mu_0 \gamma \mathbf{M} \times \mathbf{H}_{\text{eff}} + \mathbf{M} \times \frac{\alpha}{M_s} \frac{\partial \mathbf{M}}{\partial t}, \quad (4)$$

where  $M_s$  is the saturation magnetization,  $\mathbf{H}_{\text{eff}}(z)$  is the effective field (A/m),  $\gamma = 176 \text{ GHz T}^{-1}$  is the electron gyromagnetic ratio, and  $\alpha$  is the Landau–Lifshitz damping constant. Eq. (4) can be linearized assuming small perturbations from equilibrium. For harmonic regime it becomes

$$j\omega \mathbf{m} = -\mu_0 \gamma \left( M_s \hat{\mathbf{e}}_x \times \mathbf{h} - \mu_0 \gamma M_s \mathbf{m} \times \left( \frac{H_0}{M_s} \hat{\mathbf{e}}_x \right) + \left( M_s \hat{\mathbf{e}}_x \right) \times \frac{\alpha}{M_s} j\omega \mathbf{m}, \quad (5)$$

where  $\omega = 2\pi f$ ,  $\mathbf{H}_0$  and  $\mathbf{h}$  are the static and dynamic effective fields, respectively, and  $\mathbf{m}$  is the dynamic magnetization, both being complex quantities.  $\hat{\mathbf{e}}_x$  is the unit vector along the  $x$  axis. Projection of (5) along the  $y$  and  $z$  direction provides the relationship between the components of  $\mathbf{h}$  and  $\mathbf{m}$

$$\begin{pmatrix} h_y \\ h_z \end{pmatrix} = \begin{pmatrix} h_0 + j\tilde{\omega}\alpha & -j\tilde{\omega} \\ j\tilde{\omega} & h_0 + j\tilde{\omega}\alpha \end{pmatrix} \begin{pmatrix} m_y \\ m_z \end{pmatrix}, \quad (6)$$

where  $h_0 = \frac{H_0}{M_s}$  is the normalized static effective field and  $\tilde{\omega} = \frac{\omega}{\mu_0 \gamma M_s}$  is the normalized angular frequency. The  $z$ -component of the effective field in (6) is the demagnetizing field.

$$h_z = -N_{d,zz} m_z, \quad (7)$$

with  $N_{d,zz}$  the related demagnetizing factor. We disregard, in this approximation, the exchange field. By replacing  $h_z$  given by Eq. (7) in Eq. (6) we obtain that the dynamic magnetization components  $m_z$  and  $m_y$  are related by the expression

$$m_z = -\frac{j\tilde{\omega}}{(h_0 + N_{d,zz} + j\tilde{\omega}\alpha)} m_y, \quad (8)$$

which, once introduced in Eq. (6), leads to the following relationship between the dynamic longitudinal field and magnetization

$$h_y = \left( h_0 + j\tilde{\omega}\alpha - \frac{\tilde{\omega}^2}{(h_0 + N_{d,zz} + j\tilde{\omega}\alpha)} \right) m_y. \quad (9)$$

We thus obtain the complex susceptibility  $\chi(\omega)$  as

$$\chi(\omega) = \frac{m_y}{h_y} = \left( h_0 + j\frac{\omega}{\mu_0 \gamma M_s} \alpha - \frac{\left( \frac{\omega}{\mu_0 \gamma M_s} \right)^2}{(h_0 + N_{d,zz} + j\frac{\omega}{\mu_0 \gamma M_s} \alpha)} \right)^{-1} \quad (10)$$

and the complex permeability

$$\mu_{\text{int}}(\omega) = \frac{b_y}{h_y} = \mu_0 (1 + \chi(\omega)) = \mu'_{\text{int}} - j\mu''_{\text{int}}, \quad (11)$$

which plays the role of dynamic constitutive equation ( $\lim_{\omega \rightarrow 0} \mu_{\text{int}}(\omega) = \mu_{\text{DC}}$ ). Let us then consider the Maxwell's diffusion equation, governing the magnetization profile in the plate of conductivity  $\sigma$

$$\frac{\partial^2 h_y}{\partial z^2} = j\omega \sigma h_y. \quad (12)$$

Because of the symmetry of the problem,  $z$  can be restricted to

$0 \leq z \leq \frac{d}{2}$ . Eq. (12) is solved together with the constitutive Eq. (11), with the boundary conditions  $\frac{\partial h_y}{\partial z} \Big|_{z=0} = 0$  and  $\frac{\partial h_y}{\partial z} \Big|_{z=\frac{d}{2}} = \frac{d}{2} j\omega \sigma B_p$ ,

with  $B_p$  the average value of the peak induction across the sample thickness. Introducing (11) in (12) we obtain

$$\frac{\partial^2 h_y}{\partial z^2} = j\omega \sigma \mu_{\text{int}} h_y, \quad (13)$$

whose solution, under the previous boundary conditions, provides

$$h_y(z) = j\omega \sigma B_p \frac{d}{2} \frac{\cosh(kz)}{\sinh\left(k\frac{d}{2}\right)}. \quad (14)$$

The wave vector  $k$  is the solution of the characteristic equation  $k^2 - j\omega \sigma \mu_{\text{int}} = 0$  and is given by the dispersion relation

$$k = \frac{1+j}{\sqrt{2}} \sqrt{j\omega \sigma \mu_{\text{int}}} = (1+j) \frac{\lambda}{d}, \quad (15)$$

where  $\lambda$  is the complex quantity

$$\lambda = \lambda' + j\lambda'' = \sqrt{\frac{\omega \sigma |\mu_{\text{int}}|^2 d^2}{2}} \cdot \left( \sqrt{\frac{1 + \mu'_{\text{int}} |\mu_{\text{int}}|}{2}} - j \sqrt{\frac{1 - \mu'_{\text{int}} |\mu_{\text{int}}|}{2}} \right) \quad (16)$$

Since the effective field  $h_y(z)$  coincides with the applied field  $h_a(z)$  at the plate surface

$$h_{a,y} = h_y \left( \frac{d}{2} \right) = j\omega \sigma B_p \frac{d}{2} \frac{\cosh\left(k\frac{d}{2}\right)}{\sinh\left(k\frac{d}{2}\right)}, \quad (17)$$

we obtain the complex specific power as

$$\mathcal{S}(f) = \frac{1}{2} j\omega B_p h_{a,y}^* = \frac{\pi^2}{6} \sigma d^2 B_p^2 f^2 \frac{3 \coth\left(k^* \frac{d}{2}\right)}{k^* \frac{d}{2}} \quad (18)$$

with  $k^*$  the complex conjugate of  $k$ . By taking the real part of  $\mathcal{S}$ , we calculate the energy loss per cycle generated by the rotational process

$$W_{\text{rot}}(f) = \text{Re}(\mathcal{S})/f = \frac{\pi}{2} \frac{B_p^2}{|\mu_{\text{int}}|} \cdot \frac{(\lambda' - \lambda'') \sinh(\lambda' - \lambda'') - (\lambda'' + \lambda') \sin(\lambda' + \lambda'')}{\cosh(\lambda' - \lambda'') - \cos(\lambda' + \lambda'')}, [J/m^3] \quad (19)$$

with  $|\mu_{\text{int}}(f)|$  obtained via Eq. (10). Fig. 8 provides an example of application of Eq. (19) to the energy loss measured between a few Hz and 1 GHz at  $J_p = 10 \text{ mT}$  in the  $20 \mu\text{m}$  thick  $K_{\perp}$  ribbons (conductivity  $\sigma = 8.26 \cdot 10^6 \Omega^{-1} \text{ m}^{-1}$ , anisotropy constant  $K_{\perp} = 24 \text{ J/m}^3$ , Landau–Lifshitz damping constant  $\alpha = 0.04$ , demagnetizing coefficient  $N_{d,zz} = 0.786$ ). Comparison is made with the prediction offered by the standard Eq. (2), based on the solution of the Maxwell's diffusion equation with  $\mu_{\text{DC}}$  as magnetic constitutive equation. The d.w. activity, which is directly observed by Kerr experiments to expire entering the MHz range, is responsible for the hysteresis and excess dynamic loss, the difference between the measured loss  $W(f)$  and  $W_{\text{rot}}(f)$  up to such frequencies. It is apparent how the prediction by Eq. (19) accounts for the general behavior of  $W(f)$  at the highest frequencies, but for a residual difference, which is the result of the approximations involved in the analytical derivation of  $W_{\text{rot}}(f)$ . In such treatment we have disregarded, in particular, the role of the exchange field, in order to simplify the analytical procedure, thereby ignoring the restraining action of it on the skin effect, which is eventually conducive to

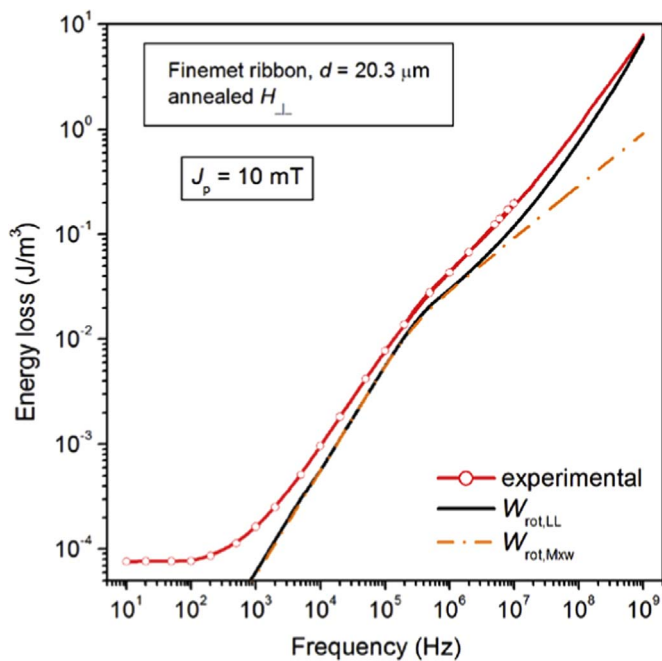


**Fig. 8.** Example of energy loss measured up to 1 GHz at  $J_p = 10$  mT in the  $K_{\perp}$  nanocrystalline ribbon and theoretical prediction of the rotational contribution using: 1) The classical model ( $W_{rot,Mxw}(f)$ ) based on the Maxwell's diffusion equation with magnetic constitutive equation defined by  $\mu_{DC}$  (Eq. (2), dashed line); 2) Modeling by coupled Landau–Lifshitz and Maxwell's diffusion equation ( $W_{rot,LL}(f)$ , Eq. (19) solid line).

higher eddy current losses.

#### 4. Conclusion

We have investigated the role of different treatments on the behavior of permeability and losses of Finemet-type nanocrystalline alloys from quasi-static excitation up to 1 GHz. They show, according to their thermomagnetic history, a variety of broadband soft behaviors, which are optimized at all frequencies in terms of magnetic losses and Snoek's product by favoring the role of moment rotations versus the d.w. displacements. Superior performances are thus brought to light in the transverse field annealed samples. It is shown that the Statistical Theory of Losses and the related concept of loss separation can provide a good theoretical framework for the experimental frequency dependence of the energy loss up to a limiting frequency ranging between some 10 kHz and a few hundred kHz. The DC permeability at the measuring peak polarization is taken in this context as a magnetic constitutive equation, an assumption justified by the necessarily involved low  $J_p$  values. The formulation of a dynamic constitutive equation, however, permitting one to theoretically cover the whole broad frequency range, is not at hand at present time, but for the most appealing case of transverse anisotropy ribbons, where the magnetization proceeds by rotations. In this case it is the Landau–Lifshitz equation that provides such an equation and one can eventually attain at a closed expression for the rotation related magnetic losses (i.e. the classical losses).

#### Acknowledgment

This research received partial support from the project KVAR (ITMS 26110230084), financed through the European Social Fund and by the project VEGA 1/0330/15 of both: the Scientific Grant Agency of the Ministry of Education, Science, Research and Sport of the Slovak Republic and the Slovak Academy of Sciences. The authors would like to thank Mr. Milan Vitovský (Vacuumschmelze GmbH & Co. KG Hanau, Germany) for providing the Vitroperm.

#### References

- [1] G. Herzer, Nanocrystalline soft magnetic alloys, in: *Handbook of Magnetic Materials*, 10, Elsevier, Amsterdam, 1997, p. 415.
- [2] F. Alves, F. Simon, S.N. Kane, F. Mazaleyrat, T. Waeckerlé, T. Save, A. Gupta, Influence of rapid stress annealing on magnetic and structural properties of nanocrystalline  $Fe_{74.5}Cu_1Nb_{3.5}Si_{15.5}B_6$  alloy, *J. Magn. Magn. Mater.* 294 (2005) e141–e144.
- [3] F. Fiorillo, E. Ferrara, M. Coisson, C. Beatrice, N. Banu, Magnetic properties of soft ferrites and amorphous ribbons up to radiofrequencies, *J. Magn. Magn. Mater.* 322 (2010) 1497–1504.
- [4] F. Mazaleyrat, L.K. Varga, Ferromagnetic composites, *J. Magn. Magn. Mater.* 215–216 (2000) 253–259.
- [5] R. Lebourgeois, S. Bérengruer, C. Ramiarinaona, T. Waeckerlé, Analysis of the initial complex permeability versus frequency of soft nanocrystalline ribbons and derived composites, *J. Magn. Magn. Mater.* 254–255 (2003) 191–194.
- [6] J. Petzold, Applications of nanocrystalline soft magnetic materials for modern electronic devices, *Scr. Mater.* 48 (2003) 895–901.
- [7] I. Betancourt, Magnetization dynamics of amorphous ribbons and wires studied by inductance spectroscopy, *Materials* 4 (2011) 37–54.
- [8] J. Füzér, S. Dobák, P. Kollár, Magnetization dynamics of  $FeCuNbSiB$  soft magnetic ribbons and derived powder cores, *J. Alloy. Compd.* 628 (2015) 335–342.
- [9] W.S. Ament, G.T. Rado, Electromagnetic effects of spin wave resonance in ferromagnetic materials, *Phys. Rev.* 97 (1955) 1558–1666.
- [10] L. Kraus, Theory of giant magneto-impedance in the planar conductor with uniaxial magnetic anisotropy, *J. Magn. Magn. Mater.* 195 (1999) 764–778.
- [11] C. Serpico, I.D. Mayergoyz, G. Bertotti, Analysis of eddy currents with Landau–Lifshitz equation as a constitutive relation, *IEEE Trans. Magn.* 37 (2001) 3546–3549.
- [12] G. Bertotti, A. Magni, I.D. Mayergoyz, C. Serpico, Landau–Lifshitz magnetization dynamics and eddy currents in metallic thin films, *J. Appl. Phys.* 91 (2002) 7559–7561.
- [13] G. Bertotti, *Hysteresis in Magnetism*, Academic Press, San Diego, CA 1998, p. 391.
- [14] F. Fiorillo, Measurements of magnetic materials, *Metrologia* 47 (2010) S114–S142.
- [15] A. Magni, F. Fiorillo, E. Ferrara, A. Caprile, O. Bottauscio, C. Beatrice, Domain wall processes, rotations, and high-frequency losses in thin laminations, *IEEE Trans. Magn.* 48 (2012) 3796–3799.
- [16] A. Magni, C. Beatrice, O. Bottauscio, A. Caprile, E. Ferrara, F. Fiorillo, Magnetization process in thin laminations up to 1 GHz, *IEEE Trans. Magn.* 48 (2012) 1363–1366.
- [17] C. Appino, G. Bertotti, O. Bottauscio, F. Fiorillo, P. Tiberto, D. Binetti, J. P. Ducreux, M. Chiampi, M. Repetto, Power losses in thick steel laminations with hysteresis, *J. Appl. Phys.* 79 (1996) 4575–4577.
- [18] S. Zirka, Y. Moroz, P. Markatos, A.J. Moses, Viscosity-based magnetodynamic model of soft magnetic materials, *IEEE Trans. Magn.* 42 (2006) 2121–2132.
- [19] O. de la Barrière, C. Appino, F. Fiorillo, C. Ragusa, M. Lecrivain, L. Rocchino, H. Ben Ahmed, M. Gabsi, F. Mazaleyrat, M. LoBue, Characterization and prediction of magnetic losses in soft magnetic composites under distorted induction waveform, *IEEE Trans. Magn.* 49 (2013) 1318–1326.
- [20] E. Barbisio, F. Fiorillo, C. Ragusa, Predicting loss in magnetic steels under arbitrary induction waveform and with minor hysteresis loops, *IEEE Trans. Magn.* 40 (2004) 1810–1819.
- [21] S. Flohrer, R. Schaefer, C. Polak, G. Herzer, Interplay of uniform and random anisotropy in nanocrystalline soft magnetic alloys, *Acta Mater.* 53 (2005) 2937–2942.
- [22] O. Bottauscio, F. Fiorillo, C. Beatrice, A. Caprile, A. Magni, Modeling high-frequency magnetic losses in transverse anisotropy amorphous ribbons, *IEEE Trans. Magn.* 51 (2015) 2800304.